

# Reinforced silicon neural microelectrode array fabricated using a commercial MEMS process

**Mohamad Hajj-Hassan**

**Vamsy Chodavarapu**

McGill University

Department of Electrical and Computer Engineering

3480 University Street

Montreal, Quebec H3A2A7, Canada

E-mail: vamsy.chodavarapu@mcgill.ca

**Sam Musallam**

McGill University

Department of Electrical and Computer Engineering

3480 University Street

Montreal, Quebec, H3A2A7

and

Department of Physiology

3655 Promenade Sir William Osler

Montreal, Quebec H3G1Y6, Canada

**Abstract.** We report the development of a silicon microelectrode array for brain machine interfaces and neural prosthesis fabricated in a commercial microelectromechanical systems (MEMS) process. We demonstrate high-aspect ratio silicon microelectrodes that reach 6.5 mm in length while having only 10  $\mu\text{m}$  thickness. The fabrication of such elongated neural microelectrodes could lead to the development of cognitive neural prosthetics. Cognitive neural signals are higher level signals that contain information related to the goal of movements such as reaching and grasping and can be recorded from deeper regions of the brain such as the parietal reach region (PRR). We propose a new concept of reinforcing the regions of the electrodes that are more susceptible to breakage to withstand the insertion axial forces, retraction forces, and tension forces of the brain tissue during surgical implantation. We describe the design techniques, detailed analytical models, and simulations to develop reinforced silicon-based elongated neural electrodes. The electrodes are fabricated using the commercial MicraGem process from Micralyne, Inc. The use of a commercial MEMS fabrication process for silicon neural microelectrodes development yields low-cost, mass-producible, and well-defined electrode structures. © 2009 Society of Photo-Optical Instrumentation Engineers. [DOI: 10.1117/1.3184795]

Subject terms: neuroMEMS; brain machine interface; neural prosthesis; elongated microelectrodes; electrode reinforcement; silicon microfabrication; MicraGem.

Paper 09020RR received Feb. 10, 2009; revised manuscript received May 21, 2009; accepted for publication Jun. 2, 2009; published online Jul. 23, 2009.

## 1 Introduction

The interfacing and interpretation of human neural systems at peripheral, spinal, and supraspinal levels, which requires the recording of the electrical activity generated by nerve cells, has been one of the core activities of neuroscience for many years.<sup>1-3</sup> The recording and processing of neural signals is required to understand how the brain processes information in response to controlling body functions. Such information could lead to successful development of closed-loop neural prostheses, which can assist paralyzed patients by allowing them to operate computers or robots with their neural activity. These prostheses typically employ microelectrodes implanted in different areas of the brain or assembled into an array that can sample a larger portion of a single area to map the brain function and dynamics of complex networks of neurons.<sup>4,5</sup> Therefore, multiple-recording-site microelectrode arrays have become a key component of neural prosthesis development, as they represent the machine to interface with the brain.<sup>3,6</sup> Given the rapid advancements in silicon micromachining technologies, there is a great interest to develop silicon-based neural microelectrodes with well-defined electrodes and precise placement of multiple recording sites on each electrode.<sup>7-10</sup> Further, there is a need for improving the

mass-production and cost-effectiveness of these technologies to increase their accessibility to large patient populations.

Cognitive control signals for neural prosthetics is a relatively new concept that deals with monitoring and understanding the messages of higher order neurons involved in planning and motivation for movements such as reaching and grasping.<sup>11,12</sup> These signals can be located in the posterior parietal reach region (PRR) located medial to the intraparietal sulcus and the dorsal premotor cortex. These regions are located much deeper in the brain compared to the motor cortex, which provides the actual control signals for movements. The PRR lies within a broader area of the posterior parietal cortex (PPC). The PPC is located functionally at a transition between sensory and motor areas and is involved in transforming sensory inputs into plans for action or so-called sensory-motor integration.

Many of the current available silicon microelectrodes cannot be effectively used to gather information from the deeper regions of the PRR because of their shorter lengths. Well-known examples of such microelectrodes include the Utah and Michigan arrays. The Utah electrode arrays are fabricated along the cross section of a silicon wafer. Consequently, the electrode length is limited by the thickness of the silicon wafer and typical probe lengths are only 1.5 mm (Ref. 13). In addition, only one electrode site can be made on every probe. The Michigan array electrodes are made of

boron-doped silicon substrates and most reported electrodes reach average lengths of 4 mm long.<sup>14,15</sup> Recently, Norlin et al.<sup>16</sup> have demonstrated 5 mm-long electrodes using deep reactive-ion-etching (DRIE) of silicon-on-insulator (SOI) substrates, and longer electrodes have been later demonstrated using the same process. The probe length is considered as one of the key requirements for the acquisition of the cognitive signals located at deeper regions in the brain. These regions are typically located deeper than 6 mm from the surface of the brain tissue in humans and in nonhuman mammals like monkeys.<sup>17</sup> Considering the length requirement, the probes also need to be supported to withstand the insertion axial forces, retraction forces, and tension forces of the brain tissue during implantation without increasing the footprint of the electrode array. Here, we propose the concept of reinforcing the regions of the electrodes that are more susceptible to breakage. We show that reinforcing specific regions of the probe with metallic layers pushes the region of maximum stress from the center to the base region of the probe, which is typically sturdier.

To date, many of the microelectrodes for neural prosthesis are fabricated using custom and individual institutional clean-room environments.<sup>18,19</sup> Here, we describe the implementation of the neural microelectrode arrays using a commercial MEMS foundry process. The use of a commercial foundry process allows development of cost-effective neural prosthesis through volume mass-production. The simplification and standardization of the development rules and processes lead to high yield, accurate reproduction, and well-defined structures. The availability of silicon (for use as the substrate material) and gold (for use as recording site material) in the standard MicraGem process from Micralyne, Inc., encouraged us to employ it for the fabrication of the described electrode array. In Sec. 2, we describe the neural probe design requirements and characteristics. In Sec. 3, we describe analytical models to understand the parameters that most govern the probe development and functionality. In Sec. 4, we provide the numerical models for the development of reinforced elongated neural electrodes. Last, in Sec. 5, the commercial microfabrication process for the neural electrodes is presented and the microfabrication results are discussed.

## 2 Microelectrode Design and Characteristics

A major criteria related to the neural microelectrode design is to have as minimal footprint as possible to minimize damage to the brain tissue and neuron networks. Typically, probe thicknesses less than  $50\ \mu\text{m}$  for silicon-based probes are preferred. The need for elongated electrode structures with lengths longer than 6 mm to gather cognitive neural information adds further complications in the design and fabrication of the microelectrodes. These electrodes should have the ability to survive the different types of forces during the insertion and retraction phases of the surgical implantation. Here, we introduce the novel concept of reinforcing the electrodes at their most susceptible regions for breakage to increase their durability. We designed probe structures with tapered chisel-shaped ends to facilitate easy entry into the brain tissue. A prototype silicon microelectrode array is fabricated using the commercial MicraGem process consisting of five electrode probes constructed with gold as the recording site material. Figure 1 shows the de-

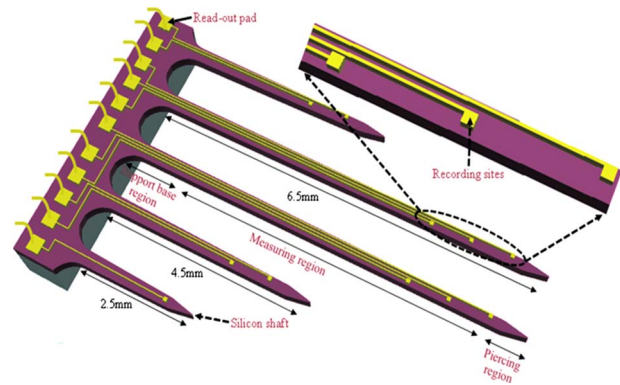


**Fig. 1** Design of the multisite elongated neural microelectrode array showing the recording sites, interconnects, and bond pads. The figure is not to scale.

sign of the proposed multi-electrode array with probes varying from 2.5 mm to 6.5 mm in length. Each probe is divided into three regions (1) support base region, (2) measuring region, and (3) piercing region. The support base region measures  $250\ \mu\text{m}$  in length, with a width of  $350\ \mu\text{m}$  at the base that rapidly reduces to a width of  $150\ \mu\text{m}$ , thus minimizing tissue damage and displacement while providing sturdy support at the base of the probe. The measuring region starts with a width of  $150\ \mu\text{m}$  at the base and ends up with  $50\ \mu\text{m}$  at the other end. The electrodes have an average width of  $100\ \mu\text{m}$  over the majority of the length of the measuring region. The measuring region has  $10\ \mu\text{m} \times 10\ \mu\text{m}$  metallic (gold) recording sites. The measuring region is followed by the piercing region, which forms the chisel-shaped tip of the probe with a length of  $250\ \mu\text{m}$  and is designed to be  $10\ \mu\text{m}$  width (minimum feature size allowed by the Micragem technology) at the end of the probe. Thus, the final taper angle is 11 deg, which is same for the different probes.

The brain is covered by the *dura mater* and the *pia mater* layers. During surgical implantation of the microelectrodes, the *dura*, which is a dense fibrous tissue, is removed. The microelectrodes are expected to pierce through the *pia*, which is a thin delicate membrane typically one cell layer thick. This layer cannot be removed for implantation due to various neurophysiological factors, and many microelectrodes crack or shatter at the *pia*. The designed microelectrode array measures  $10\ \mu\text{m}$  at the reinforced tip of each probe to increase the piercing strength. In the next section, we describe the analytical analysis used to study and understand the mechanical behavior of the probe when it is subjected to different types of forces during insertion into the brain and ultimately understand the factors that would aid in the development of reliable, functional, and elongated neural microelectrodes.

## 3 Analytical Modeling of Neural Probe Mechanics

The main forces that act upon the electrode probe during handling and insertion into the brain tissue are (1) the bending force, as illustrated in Fig. 2(b), which occurs under an out-of-plane loading causing parallel displacement to the tissue plane; and (2) the buckling force, as illustrated in

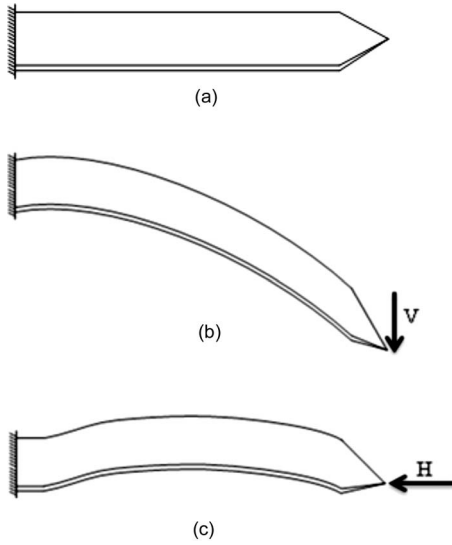


**Fig. 2** Illustration of neural probe deflections during the insertion phase (a) without deflection, (b) bending, and (c) buckling.

Fig. 2(c), which occurs under axial compression and is mainly represented by the force that counteracts the normal force exerted on the brain tissue by the probe and the shear force that prevents the tip of the probe from slipping on the surface of the brain tissue. Knowing the maximum bending force is important, as it determines the maximum out-of-plane force at which breakage of the probes can occur. A case in which this transverse bending occurs is when moving the base region of the probe after its tip region is inserted into the brain tissue. Once a bending force is applied to the tip region, the electrode deflects in a quarter-circle way, as depicted in Fig. 2(b), causing a maximum (above normal) stress at the fixed bottom of the probe connected to the base holding the bonding pad and an average (normal) stress at the middle region of the probe. These stresses are given by Eqs. (1) and (2).<sup>20</sup>

$$\sigma_{\max} = \frac{3Et\delta}{2L^2}, \quad (1)$$

$$\sigma_{\text{Avg}} = \frac{3Et\delta}{4L^2}, \quad (2)$$

where  $L$  is the probe length,  $t$  is the thickness,  $E$  is the Young's modulus of silicon, and  $\delta$  is the maximum deflection at the probe tip. The maximum bending force, which the probe can withstand at the tip region without breaking, is derived from the basic differential equation for the deflection curve of a suspended beam fixed at one end and free to move at the other end. It is given by Eq. (3):<sup>21</sup>

$$P_{\max} = \frac{\sigma_{\max} W t^2}{6L}, \quad (3)$$

where  $W$  is the width of the probe at the base, and  $\sigma_{\max}$  is the maximum stress of the electrode. The maximum bending force,  $P_{\max}$ , is still valid to be applied for both uniform cross-sectioned and gradually tapered cantilevers, as in

both cases  $P_{\max}$  depends only on the length and the cross-section dimensions at the base. The bending stiffness, however, depends on the shape of the cross section throughout the tapered probe and can be expressed by a spring constant,  $K$ , which relates the lateral deflection of the tip,  $\delta$ , relative to the transverse load,  $P$ , applied at the tip of the probe. The value for the spring constant,  $K$ , can be derived from the classical beam equation for the case in which the area moment of inertia,  $I(x)$ , of the cross section varies linearly along the probe length as given by Eq. (4):

$$EI(x) \left( \frac{d^2y}{dx^2} \right) = M(x), \quad (4)$$

where the bending moment is given by:

$$M(x) = P(x - a), \quad (5)$$

and

$$I(x) = IR \left( \frac{x}{a} \right), \quad (6)$$

where  $R$  is the ratio of the width at the tip and the width at the base, and  $I$  is the moment of inertia at the base

$$I = \frac{Wt^3}{12}. \quad (7)$$

Hence, the spring constant is given by Eq. (8):<sup>22</sup>

$$K = \frac{P}{\delta} = \frac{EW}{4} \left( \frac{t}{L} \right)^3 \left[ \frac{\left( \frac{2}{3} \right) (1 - R)^3}{(1 - R)^2 - 2R(1 - R) - 2R^2 \ln R} \right]. \quad (8)$$

In Eq. (8), the expression before the square brackets is the spring constant for a probe with uniform cross section throughout the length of the probe from the base to the tip. The expression within the square brackets represents the reduction in stiffness due to the tapering width.

The second type of force acting on the probe is the buckling force that occurs under axial compression. The buckling load is a critical parameter, as it determines the force at which the probe tip penetrates the brain tissue. For the case of insertion of the probe in brain tissue, the applied force is assumed to be axial, and the electrode probes are modeled as rigidly supported on one end (base region) and free to rotate at the other end (tip region). The axially loaded tapered probe loses its initial stable shape when it is subjected to an external force,  $P$ , greater than critical load,  $P_{cr}$ , required to buckle the single probe. For a probe with constant cross section, the governing differential equation of an axially loaded probe along the longitudinal axis, ( $x$ ), is given by Eq. (9):

$$\frac{d^2\delta(x)}{dx^2} + \frac{P_b}{EI} \delta(x) = 0, \quad (9)$$

where  $\delta$  is the transversal displacement, and  $EI$  represents the flexural rigidity of the probe. The maximum load (force) required to buckle the probe (i.e., buckling or Euler's load) is obtained by solving Eq. (9) for a probe with

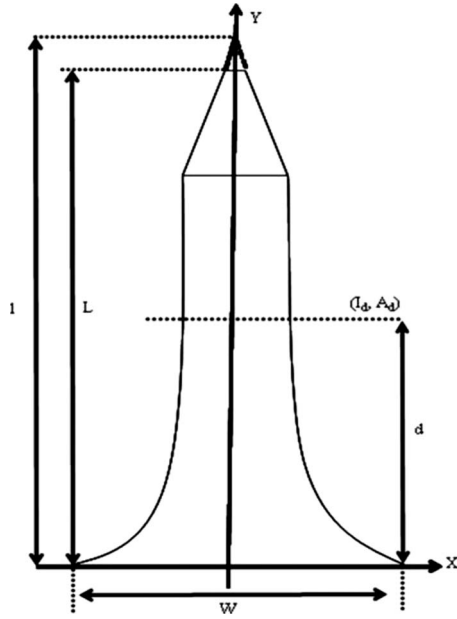


**Fig. 3** Geometric diagram of a single tapered probe electrode.

constant cross section throughout the length of the probe. It is given by Eq. (10):<sup>23</sup>

$$P_{cr} = \left( \frac{n\pi}{L} \right)^2 EI, \quad (10)$$

where  $n$  is the buckling mode,  $L$  is the length of the probe, and  $EI$  is the flexural rigidity of the probe. In order for the probe to be inserted successfully into the brain tissue without breaking, insertion should be done within the force range of the buckling strength. Inserting the probe with a force beyond the buckling strength will cause the probe to bend more, and then a mean minimal force perpendicular to the brain tissue will be exerted such that the probe will not penetrate the brain tissue.

In the case of a tapered probe, a probe with varying cross section along its length from the probe base toward its tip, as depicted in Fig. 3, Eq. (10) depends on the variable in longitudinal direction stiffness factor  $EI(y)$ . Therefore, the law of distribution of the moment of inertia of a cross section along the length of the probe may be presented by Eq. (11):

$$I(d) = I_b \left\{ 1 - (1 - k^2) \frac{d}{L} \right\}^m, \quad (11)$$

where  $d$  is a distance from the probe base section, with a cross-section area  $A_b$  and a moment of inertia  $I_b$ , to any considered section, with a cross-section area  $A_d$  and a moment of inertia  $I_d$ . The factor  $k^{2m}$  in Eq. (11) is given by Eq. (12):

$$k^{2m} = \frac{I_d}{I_b}, \quad (12)$$

where  $m$  is a factor of the longitudinal distribution of the second moment of area, which can be changed as  $m=1, 2,$

3, or 4 depending on the cross-sectional type. For instance, for  $m=0$ , we obtain a probe of constant cross section; for  $m=2$ , we obtain a pyramidal probe; for  $m=3$ , we get a hollow cone, and for  $m=4$ , a solid cone, etc. The differential equation of the tapered probe, as proposed by Dinnik,<sup>24</sup> is represented in Eq. (13):

$$EI \left[ 1 - (1 - k^2) \frac{d}{l} \right]^m y'' + Py = 0, \quad (13)$$

where  $l$  is a distance from the bigger end of the probe section up to a fictional point along the length probe where the second moment of cross-section area tends to zero. In this case, Eq. (13) can be solved in terms of Bessel's functions<sup>25</sup> and may be presented as Eq. (14):

$$P = S \frac{EI}{l^2}, \quad (14)$$

where  $S$  is the coefficient of stability, depending on variability of the probe geometry and the mode of buckling. The values of  $S$  for different ratios of  $I_t/I_b$  were previously reported in Ref. 24.

Effective microelectrode design must be concerned with a trade-off between the conflicting requirements of a small diameter to minimize tissue damage and a large diameter to minimize buckling. To resolve these two factors, it is necessary to determine the critical buckling load, which is a function of the electrode geometry and material properties relative to the maximum anticipated forces applied to the electrode during insertion into the brain. Jensen et al.<sup>26</sup> performed *in vivo* electrode insertions into the cerebral cortex of rats and found that the maximal penetration force for an array of five ACREO Inc. electrodes to be  $(2.42 \pm 0.77 \text{ mN})$ . Therefore, the present designed reinforced electrodes must withstand at least this force when penetrating the brain tissue.

#### 4 Numerical Modeling of Reinforced Electrodes

We detail studies to determine the reliability of the elongated neural probes as they are subjected to significant stresses due to imperfect insertion into the brain and/or due to movement of the brain relative to the skull. The main goals of the simulations are to predict the behavior of the probes when they are subjected to a downward bending force and an axial force, as depicted in Figs. 2(b) and 2(c), respectively. We show the simulated performance of proposed elongated probes, with and without structural reinforcement (tip displacement, stiffness, critical load point, etc.), to fulfill the requirements for gathering cognitive neural information.

For simulations, two types of forces were applied, a vertical force ( $V$ ) applied in the vertical direction at the face of the probe tip and an axial force ( $H$ ) applied horizontally at the cross section of the probe. These simulations are carried out to determine the maximum bending and buckling loads, respectively. The loads were obtained at the point where the maximum stresses at weak regions of the probe reach 1 GPa, which is near the fracture stress limit for a thin silicon cantilever.<sup>27</sup> In the case of the bending force, the maximum value of stress in the probe is located at the bottom region, and an average stress value is in the middle

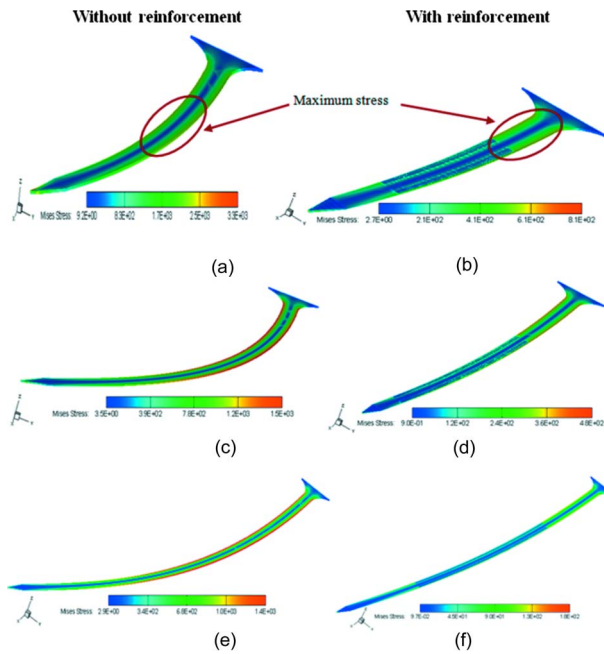


**Fig. 4** Behavior of the 2.5-mm [(a), (b)], 4.5-mm [(c), (d)], and 6.5-mm [(e), (f)] probes, without and with reinforcement, respectively, when they are subjected to axial horizontal force.

region (Fig. 4), while in the case of an axial force, the maximum stress in the probe is in the middle region and an average stress value is present at the bottom region. The maximum average out-of-plane bending load, which causes the probe to be broken, and the maximum average in-plane buckling force for different lengths of the probes as determined by simulations using CoventorWare software tool,<sup>28</sup> are summarized in Table 1. Here, the place of reinforcement was selected based on the simulations, which show that the weaker region susceptible to breakage is located at the middle of the probe. The reinforcing structures are placed exactly at the middle of the probe, with an average width of 25 microns. The reinforcing structures were placed 5 microns away from the interconnections in order to respect the design rule of the MicraGem process technology. The length of the reinforcement is as follows: 1 mm length for the 2.5-mm electrode, 2 mm length for the 4.5-mm electrode, and 3.5 mm length for the 6.5-mm electrode.

**Table 1** Comparative buckling simulation results of different lengths of the reinforced and nonreinforced electrodes.

Electrode	Critical buckling load (without reinforcement)	Critical buckling load (with reinforcement)	Critical vertical loading (with reinforcement)
6.5 mm	0.575 N	0.724 N	0.085 N
4.5 mm	0.8505 N	0.971 N	0.1449 N
2.5 mm	0.975 N	1.23 N	0.1653 N

As shown in Eqs. (3) and (14), the critical bending and buckling loads are dependent on the thickness of the probe. Therefore, the stability of the probe always can be improved by increasing its thickness, but such a design will increase the damage of the brain tissues during implantation of the probe. Further, commercial MEMS processes typically have fixed thickness for the silicon layer, as in the case of MicraGem process, which will not allow increasing the silicon probe thickness. A better solution is obtained by keeping the same thickness of the probe as small as possible and increasing the stability by introducing reinforcing structures. In the case of an axially compressed probe, as shown in Fig. 2(c), its stability can be made greater by adding a stiff longitudinal reinforcing structure of suitable cross section. The volume of such a reinforcement structure will be much smaller than the additional volume introduced by an increasing the probe thickness.

In our present application, the horizontal force component is very important as it determines the force at which the probe tip penetrates the brain tissue. Therefore, it is important to reinforce the probe at the middle because for this kind of force load the maximum stress is in the middle of the probe where the probe is the most susceptible for breakage. The design of our new reinforced probe is structurally similar to the standard probe but with additional metal layers added to strengthen its weaker areas—that is, at the middle of the probe. The dimension of the reinforcement is provided earlier. The reinforcement of the probes increased its tensile strength when compared to the standard probe by pushing back the maximum stress in the middle to the bottom region of the probe, which is typically sturdier, as shown in Fig. 4. This enables the probe to be more resistant to the axial buckling force exerted by the brain tissue during the implantation phase.

### 5 Microelectrode Fabrication and mechanical testing

The developed neural electrode array consists of five probes fabricated using the standard MicraGem process from Microlyne, Inc.,<sup>29</sup> made available through the Canadian Microelectronics Corporation (CMC). Figure 5 illustrates the steps of the MicraGem fabrication process. The process starts with a  $500 \pm 25\text{-}\mu\text{m}$ -thick glass (Pyrex) wafer, which is patterned and isotropic wet etched, as depicted in Fig. 5(a), to form a cavity that is used to suspend the probes. Then, a silicon-on-insulator (SOI) wafer is turned device layer down and anodic bonded to the patterned glass substrate, as depicted in Fig. 5(b). The silicon handle and buried oxide layers are then etched away completely using a wet etch process, leaving behind the exposed single-crystal silicon layer (device layer) bonded to the glass, as illustrated in Fig. 5(c). The developed probes are made of this single-crystal silicon layer, which is  $10\ \mu\text{m}$  thick. Metal layers are then deposited over the single-crystal silicon surface consisting of  $500\text{-}\text{\AA}$ -thick titanium-tungsten, as an adhesion layer, and a  $2000\text{-}\text{\AA}$ -thick gold layer. The metal layers are lithographically patterned and then wet etched to form the recording pads, trace lines (interconnects), bonding pads, and the reinforcing layer, as depicted in Fig. 5(d). Last, the single-crystal silicon layer is lithographically patterned and then etched completely using a DRIE process to form the electrode probes, as illustrated in

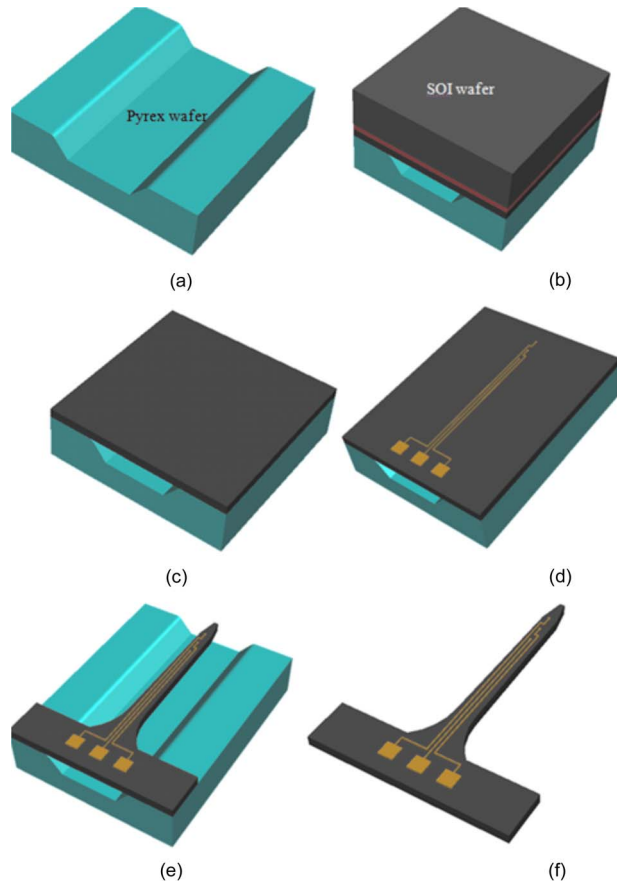


**Fig. 5** Schematic illustration of the standard MicraGem microfabrication process.

Fig. 5(e). The electrode structures are released from the Pyrex support with a post-fabrication process step by etching the intermediate silicon dioxide layer, formed during the anodic bonding of the SOI wafer to the Pyrex wafer, using buffered hydrofluoric acid, as illustrated in Fig. 5(f).

The microelectrode array can be later encapsulated using Parylene-C as a biocompatible layer in a postfabrication process step for surgical implantation with only the recording sites exposed to the neurons.<sup>30</sup> The complete fabricated sample is shown in Fig. 6(a). Figure 6(b) shows a magnified view of the reinforced probe tip and one of the recording sites. Figures 6(c) and 6(d) show reinforced and nonreinforced electrodes, respectively. The recording sites and interconnections are also shown in these figures. These structures are made of low-stress metal deposited with low average residual stress that provides long-term reliability. The silicon and metal structures shown in Fig. 6 are well defined and uniform, which is characteristic of the commercial MEMS process.

A successful penetration of the neural probe electrodes into brain tissue occurs with no breakage or excessive dimpling. Hence, it is important to analyze and define the operational limits of the silicon-based neural microelectrodes. The predefined limit to which the electrodes can be stressed is often referred to as the buckling load, which represents the maximum allowable compressive loads that the probe electrodes are capable of withstanding without failure. We

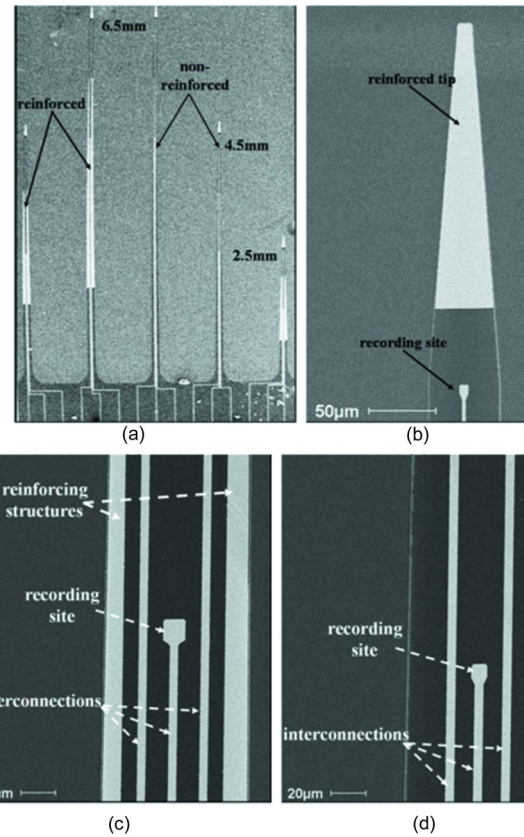


**Fig. 6** SEM photos of the fabricated array using the standard MicraGem process: (a) probe array, (b) tip of the electrode, (c) reinforced electrode at the middle region, and (d) nonreinforced electrode.

performed experimental evaluation to determine the mechanical stability of the neural electrodes by determining the critical buckling load. The fabricated neural electrode array has five probes with one probe of 2.5 mm length, two probes of 4.5 mm length, and two probes of 6.5 mm length (Fig. 1). In order to compare the critical loads of the reinforced and nonreinforced probe electrodes, the fabricated sample includes one 4.5-mm-long and one 6.5-mm-long electrode that are reinforced; the other two of the same lengths are left nonreinforced. In our application, the probe electrodes can be treated as cantilever beams that are fixed at the base end and free to move at the tip end. When a critical load is applied, buckling occurs in the plane perpendicular to the corresponding principal axis of inertia. The critical loads are calculated by buckling the probe electrodes, as illustrated in Fig. 2(c), until the electrodes break and by measuring the maximum deflection,  $d_{max}$ . Equations (15) and (16) were used to calculate the critical stress  $\sigma_{cr}$  (Ref. 31). The critical stress is then used to find the critical load,  $P_{cr}$ , of the beam being loaded:

$$d_{max} = \frac{\sigma_{cr} L^2}{6Et}, \quad (15)$$

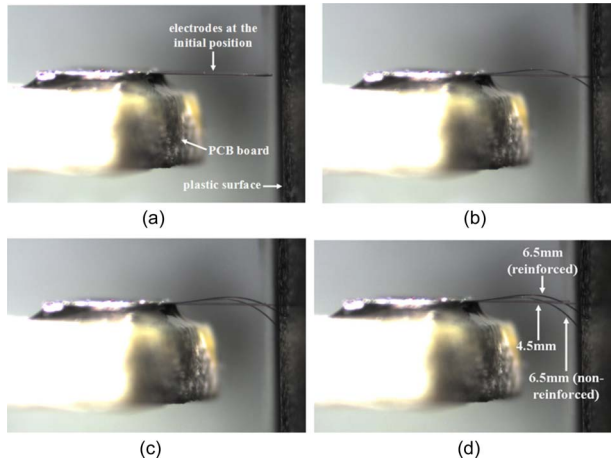


**Fig. 7** Buckling testing of probe electrodes when pressed against a hard plastic surface.

$$P_{cr} = \sigma_{cr} A, \quad (16)$$

where  $E$  is the elastic modulus for silicon and is assumed to be 190 GPa (Ref. 32),  $t$  is the probe electrode thickness, and  $L$  is effective length, which is equal to one half the actual length of the probe electrode as it is determined by the method of support.<sup>31</sup>

In this experiment, a horizontal loading setup was used for the buckling studies. The test platform consists of the electrode array mounted and glued on a custom-designed printed circuit board using an epoxy material to allow easy handling of the array during the test procedure, as shown in Fig. 7(a). The PCB board is then mounted on a motion controller to allow slow advancement of the probe electrodes in small and accurate steps. Figure 7(a) shows the electrodes in the initial load phase as pressed against a hard plastic surface. As the electrodes moved forward and pressed against the hard surface, the deflection of the electrodes increased. Figures 7(b)–7(d) provide a visual explanation of the buckling experiment where the nonreinforced electrodes of both 6.5 mm and 4.5 mm lengths deflect and buckle more than the reinforced electrodes of the same length. The values of maximum deflections  $d_{max}$  of the reinforced and nonreinforced electrodes were measured at the last point before fracture using a microscope and a micrometer grid. Based on the stress deflection Eqs. (15) and (16) described previously, the critical stress of the reinforced and nonreinforced probe electrodes as they are pressed against the hard surface were calculated, as summarized in Table 2. The buckling experiment was repeated three times for three different arrays, and there was no statistically significant difference in the results. The measured critical buckling loads are in good agreement with the simulation results. The probes are currently undergoing *in vivo* testing in rat cerebral cortex.

## 6 Conclusions

We demonstrated a silicon microelectrode array for brain machine interfaces fabricated in a commercial MEMS process available from Micalyne, Inc. The use of standard fabrication processes yields mass-producible and well-defined probe structures. We presented the design, analyti-

**Table 2** Comparative buckling test results of different lengths of the reinforced and nonreinforced electrodes.

Electrode	Measured critical buckling load (without reinforcement)	Measured critical buckling load (with reinforcement)
6.5 mm	0.561 N	0.717 N
4.5 mm	0.847 N	0.976 N
2.5 mm	—	1.193 N

cal, and numerical models to study the stress and deflection of neural microelectrodes during various scenarios of surgical implantation and usage. We demonstrated elongated silicon microelectrodes that are up to 6.5 mm in length with only 10  $\mu\text{m}$  thickness that are suitable to gather cognitive neural information from deeper regions of brain. We described a new concept of reinforcing the regions of the microelectrodes that are more susceptible to breakage to enhance their stiffness, durability, and functionality in order to serve as optimal implantable microstructures for integrated brain machine interfaces.

## Acknowledgments

We would like to acknowledge the financial support given by the Natural Sciences and Engineering Research Council of Canada (NSERC), Le Fonds Québécois de la Recherche sur la Nature et les Technologies (FQRNT), and the Canadian Institutes for Health Research (CIHR). We would also like to thank CMC and Micalyne for providing access to the fabrication resources.

## References

1. M. R. Bear, B. W. Connors, and M. A. Paradiso, *Neuroscience Exploring the Brain*, 2nd ed., 888 p., Lippincott Williams and Wilkins, Baltimore (2001).
2. M. A. L. Nicolelis, "Brain-machine interfaces to restore motor function and probe neural circuits," *Nat. Rev. Neurosci.* **4**(5), 417–422 (2003).
3. R. C. Gesteland, B. Howland, J. Y. Lettvin, and W. H. Pitts, "Comments on microelectrodes," *Proc. Institute Radio Engineers*, **47**(11), 1856–1862 (1959).
4. M. A. L. Nicolelis, *Methods for Neural Ensemble Recordings*, CRC-Press, New York (1998).
5. S. A. Deadwyler and R. E. Hampson, "The significance of neural ensemble codes during behavior and cognition," *Annu. Rev. Neurosci.* **20**, 217–244 (1997).
6. K. Frank and M. C. Becker, "Microelectrodes for recording and stimulation," *Physical Techniques in Biological Research*, Vol. **5**, pp. 23–88 (1964).
7. K. Najafi, "Micromachined systems for neurophysiological applications," in *Handbook of Microlithograph, Micromachining, and Microfabrication, Vol. II: Micromachining and Microfabrication*, Monograph, London (1997).
8. K. D. Wise, J. B. Angell, and A. Starr, "An Integrated-Circuit Approach to Extracellular Microelectrodes," *IEEE Trans. Biomed. Eng.* **Bm17**(3), 238–247 (1970).
9. G. A. Urban, O. Prohaska, and F. Olcaytug, *Early Biomems Multi-Sensor Neuroprobes in BioMEMS*, G. A. Urban, Ed., Springer Chicago (2006).
10. D. Banks, D. J. Ewins, W. Balachandran, and P. R. Richards, "Microengineered interfaces with the nervous system," in *Medical Applications Microeng.*, IEE Colloquium on, p. 4/1–4/3 (1996).
11. S. Musallam, B. D. Corneil, B. Greger, H. Scherberger, and R. A. Andersen, "Cognitive control signals for neural prosthetics," *Science* **305**(5681), 258–262 (2004).
12. B. Pesaran, S. Musallam, and R. A. Andersen, "Cognitive neural prosthetics," *Curr. Biol.* **16**(3), R77–R80 (2006).

13. K. E. Jones, P. K. Campbell, and R. A. Normann, "A glass silicon composite intracortical electrode array," *Am. Ceram. Soc. Bull.* **20**(4), 423–437 (1992).
14. K. Najafi, K. D. Wise, and T. Mochizuki, "A high-yield ic-compatible multichannel recording array," *IEEE Trans. Electron Devices* **32**(7), 1206–1211 (1985).
15. Q. Bai, K. D. Wise, and D. J. Anderson, "A high-yield microassembly structure for three-dimensional microelectrode arrays," *IEEE Trans. Biomed. Eng.* **47**(3), 281–289 (2000).
16. P. Norlin, M. Kindlundh, A. Mouroux, K. Yoshida, and U. G. Hofmann, "A 32-site neural recording probe fabricated by DRIE of SOI substrates," *J. Math. Psychol.* **12**(4), 414–419 (2002).
17. R. A. Andersen and C. A. Buneo, "Intentional maps in posterior parietal cortex," *Annu. Rev. Neurosci.* **25**, 189–220 (2002).
18. D. Banks, "Neurotechnology," *Eng. Sci. Educ. J.* **7**(3), 135–144 (1998).
19. M. Hajj Hassan, V. Chodavarapu, and S. Musallam, "NeuroMEMS: neural probe microtechnologies," *Sensors* **8**(10), 6704–6726 (2008).
20. F. V. Warnock and P. P. Benham, *Mechanics of Solids and Strength of Materials*, Pitman, London (1965).
21. J. M. Gere and S. P. Timoshenko, *Mechanics of Materials*, PWS-KENT, Boston (1990).
22. K. A. Moxon, S. C. Leiser, G. A. Gerhardt, K. A. Barbee, and J. K. Chapin, "Ceramic-based multisite electrode arrays for chronic single-neuron recording," *IEEE Trans. Biomed. Eng.* **51**(4), 647–656 (2004).
23. S. P. Timoshenko, *Theory of Elastic Stability*, 2nd ed., McGraw-Hill, New York (1961).
24. A. N. Dinnik, "Design of columns of varying cross sections," *Trans. ASME* **51**, 105–114 (1929).
25. G. N. Watson, *Theory of Bessel's Functions*, Cambridge University Press, Cambridge, UK (1922).
26. W. Jensen, K. Yoshida, and U. G. Hofmann, "In vivo implant mechanics of flexible, silicon-based ACREO microelectrode arrays in rat cerebral cortex," *IEEE Trans. Biomed. Eng.* **53**(5), 934–940 (2006).
27. C. J. Wilson and P. A. Beck, "Fracture testing of bulk silicon microcantilever beams subjected to a side load," *J. Microelectromech. Syst.* **5**(3), 142–150 (1996).
28. CoventorWare, <http://www.coventor.com>.
29. Micralyne, <http://www.micralyne.com/>.
30. S. Musallam, M. J. Bak, P. R. Troyk, and R. A. Andersen, "A floating metal microelectrode array for chronic implantation," *J. Neurosci. Methods* **160**(1), 122–127 (1990).
31. K. Najafi and J. F. Hetke, "Strength characterization of Silicon Microprobes in Neurophysiological tissues," *IEEE Trans. Biomed. Eng.* **37**(5), 474–481 (1990).
32. G. L. Pearson, W. T. Read, and W. L. Feldmann, "Deformation and fracture of small silicon crystals," *Acta Metall.* **5**(4), 181–191 (1957).



**Mohamad Hajj-Hassan** received his BEng and MS in biomedical engineering from Islamic University of Lebanon and Ecole Polytechnique de Montreal in 2003 and 2006, respectively. He is a PhD candidate in the Department of Electrical and Computer Engineering at McGill University. He is working on integrated CMOS-MEMS microsystems for neuroscience applications in the Sensor Microsystems Laboratory at McGill.



**Vamsy Chodavarapu** obtained his MS and PhD degrees in electrical engineering from the University at Buffalo, The State University of New York, in 2003 and 2006 respectively. He obtained his BEng degree in instrumentation engineering from Osmania University, India, in 2001. In 2006, he joined the Department of Electrical and Computer Engineering at McGill University as an assistant professor, where he directs the Sensor Microsystems Laboratory. His specific

research interests are in the areas of CMOS sensor microsystems, biological/chemical sensors, mixed-signal VLSI design, nanomaterials, and MEMS/Microfluidics. His research is funded by various government and private sources. He is a member of IEEE and SPIE.



**Sam Musallam** is an assistant professor in the Department of Electrical and Computer Engineering and an associate member of the Department of Physiology, both at McGill University, Montreal. He leads the Neural Prosthetics Laboratory at McGill University, which investigates the neuroscientific aspects of developing optimal neural prosthetic devices, and also develops implantable devices for measurement of biological signals in the brain and body.